01

Low pressure DBD in He−Ne mixture. Spectroscopy of the Afterglow

© V.A. Ivanov

St. Petersburg State University,
198504 St. Petersburg, Russia

e-mail: v.a.ivanov@spbu.ru

Received December 24, 2021
Revised February 13, 2022
Accepted April 6, 2022

The paper considers the possibility of using a low-pressure dielectric barrier discharge (DBD) as a plasma source for the active medium of a He−Ne-laser. The results of a spectroscopic study of the decay stage of a DBD plasma of a cylindrical configuration with a pronounced inverse population of the upper level of the $2p^5 5s$ configuration, which makes the line of 632.8 nm one of the brightest in the visible region of the spectrum, are presented. Based on the analysis of data on the populations of the excited levels of the neon atom and the metastable levels of helium 2^1S_0 and 2^3S_1, it is shown that in the early stage of the DBD afterglow at helium pressures of a fraction of a Torr, the distribution of populations over the $2p^5 5s$ and $2p^5 4d$ levels of the neon atom, which is characteristic of the excitation transfer mechanism, is realized. In the late afterglow with the departure of helium atoms $He2^1S_0$, emission in the visible region of the spectrum is formed mainly by transitions from levels of the $2p^5 3p$, configuration, the population of which is associated with $He(2^3S_1)$ atoms. At this stage, the population of the $2p^5 5s$ and $2p^5 4d$ states by electron-ion recombination processes is ineffective and does not lead to the formation of population inversion. As an optimal solution in terms of the 632.8 nm line brightness in the afterglow, it is proposed to use a discharge with electrodes along the outer surface of a cylindrical discharge tube, initiated at frequencies that exclude the recombination stage of the afterglow.

Keywords: elementary processes, barrier discharge, inverse population, afterglow, helium-neon plasma, excitation transfer

DOI: 10.21883/EOS.2022.07.54719.3076-21

Introduction

Dielectric barrier discharge has been used actively in recent decades in a wide range of technological applications [1,2] (including experimental optics problems of optimization of quantum generators [2] and radiation sources based on excimer molecules [2,3]). The cited reviews present successful cases of application of DBD under pressures ranging from several tens of Torr to atmospheric pressure and at frequencies ranging from several tens of kilohertz to tens of megahertz. In the present study, we turned to the spectroscopic examination of barrier discharge plasma in a He−Ne mixture with the purpose of identifying the conditions of formation of an inverse population of excited states of a neon atom in its afterglow.

Hundreds of experimental and theoretical studies focused on the processes occurring in He−Ne plasma as an active medium of the historically first gas laser [4,5] have already been published (some of them were mentioned in reviews [6,7]). This research provided a detailed insight into the mechanisms shaping the optical properties of this plasma. However, recent studies indicate that the potential of He−Ne plasma as a source of new optical phenomena is far from being exhausted. For example, it was demonstrated in [8,9] that the afterglow of a discharge in a He−Ne mixture is formed under certain conditions as a result of recombination of heteronuclear $HeNe^+$ ions ans electrons. The effect of concentration of emission of the $2p^5 4p$ shell of a neon atom, which is represented by a set of 30 spectral lines of comparable intensity in pure neon plasma, into a single line at 352.0 nm emitted from the upper $3p_1$ level (in the Paschen notation) at higher helium pressures was described in [10]. This phenomenon was discovered in studies of the evolution of the afterglow spectrum of a barrier discharge with a low neon content (several mTorr) under a total pressure of 0.1−20 Torr of the mixture. A large set of experimental data on the spectral composition and the temporal characteristics of afterglow of an extended barrier discharge of a cylindrical configuration with electrodes on the outer surface of a glass tube was obtained to interpret the observed effect (a finalized model will be presented in subsequent studies). The results of analysis of afterglow spectra added new information to the data already available for infrared transmissions [4]: inverse population of the upper level of the $2p_4 \leftarrow 3s_2$ transition emitting the 632.8 nm line is observed in a wide range of variation of pressure, composition of the He−Ne mixture, and density of plasma electrons and at different afterglow stages. This information, its interpretation, and a discussion into the possibility of constructing a He−Ne laser based on the barrier discharge are the subject matter of the present paper.

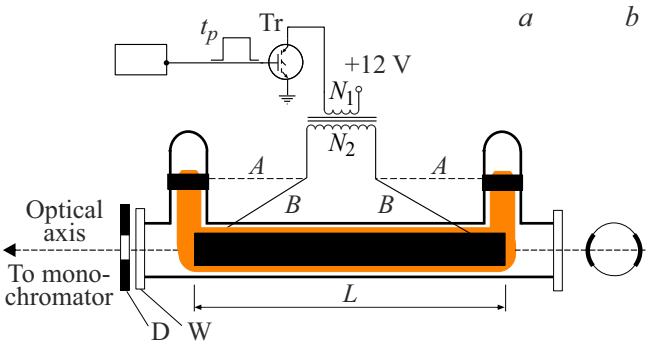

Figure 1. (a) Discharge tube (the inner diameter is 3.9 cm, $L = 22$ cm. D is an aperture 5 mm in diameter, W are quartz windows, and $A-A$ are electrodes on vertical extensions. (b) Positioning of electrodes $B-B$ on the side surface of the tube.

Experiment

We used two versions of periodic barrier discharge with the same supply circuit shown in Fig. 1. This simple circuit (see details in [11,12]) utilizes the ability of a flyback transformer to store energy in the active phase (when the transistor is on and an electrode voltage of $12(N_2/N_1)$ V is insufficient to generate discharge current) and transfer it to the secondary circuit on termination of the pulse t_p. In the considered experiment, the ratio of numbers of turns is $N_2/N_1 = 10$, and the maximum collector–emitter transistor voltage is 600 V. The circuit with these parameters provided an opportunity to examine barrier discharges of each configuration with electrode voltages up to 6000 V under helium pressures ranging from a fraction of a Torr to several tens of Torr. The current of such discharges [11] has the form of two half-waves of different polarities with a duration of $2-3\,\mu$s and a zero mean value. The emission of a discharge was observed along its axis using a monochromator with a linear dispersion of 0.6 nm/mm. The radial radiation' distribution was studied by scanning the tube image along the entrance slit of the monochromator with aperture D removed (Fig. 1). Light fluxes were detected using the method of multichannel photon count with a temporal resolution down to 40 ns.

The experimental data discussed below, which characterize the processes in decaying plasma of the He–Ne mixture, correspond to a helium pressure of 0.7 and 6.8 Torr and a neon pressure lower than 5 mTorr. The discharge glow, which characterizes the spatial parameters of a discharge, is represented by the spectral line of atomic neon at 585.2 nm emitted by pure neon plasma under a pressure of 0.9 Torr.

The densities of helium atoms in metastable states 2^1S_0 and 2^3S_1 were calculated based on the results of measurement of absorption of emission from an auxiliary source (hollow-cathode microdischarge in helium at the wavelengths of 501.57 nm ($2^1S \leftarrow 3^1P$) and 388.9 nm ($2^3S \leftarrow 3^3P$, respectively) in the near-axis tube region. In calculations, the profiles of emission and absorption lines were assumed to be Doppler ones with the complex structure of the 388.9 nm line taken into account. The method of absorption measurement of densities of metastable atoms was similar to the one detailed in [13].

The relative populations of excited levels of a neon atom in the afterglow were determined based on the plasma emission spectra in the wavelength range of 350–750 nm measured using the photon count method.

Electrons were „heated" by a pulsed high-frequency field to analyze the nature of formation of excited neon and helium atoms at the stage of plasma decay. The procedure of such an experiment was detailed in [12].

Results and discussion

The spatial distributions of densities of emitting atoms along and across the discharge tube ($A-A$ and $B-B$, Fig. 1) form in significantly different ways, but this difference has no effect on the fundamental result: population inversion is observed in the afterglow of both discharges. However, in our view, the transverse discharge has an advantage in that its initiation requires a significantly lower electrode voltage, which also depends only weakly on length L of the discharge tube, thus allowing for a wide range of L variation with no complicating modifications to the supply circuit. The results presented below corresponded to plasma with electrodes on the side surface of the discharge tube. Its emission at a wavelength of 585.2 nm (transition $1s_2 \leftarrow 2p_1$ in a neon atom) at the discharge and early afterglow stage is shown in Fig. 2. Two „humps" are formed by the discharge current half-waves mentioned above. Each half-wave produces a plasma formation with its glow maximized near the electrode that acts as a cathode in a given half-wave. Specifically, curve *1* in Fig. 3 (cathode is on the right) characterizes the radial distribution of intensity of the 585.2 nm line in the first half-wave from Fig. 2, while curve *2* corresponds to

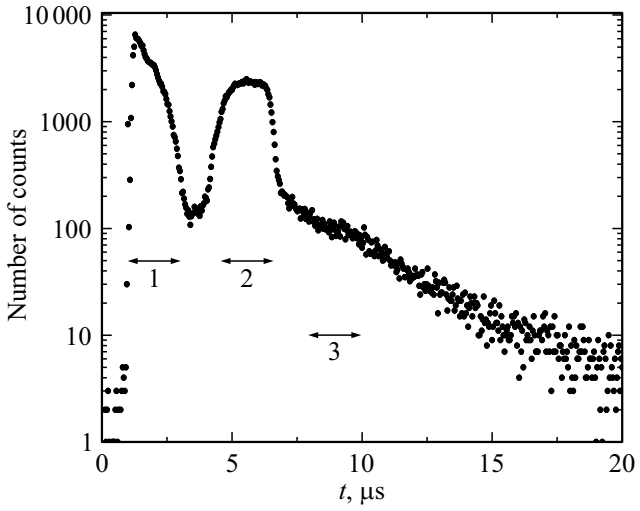

Figure 2. Intensity of the 585.2 nm line of a neon atom in a discharge in pure neon in the early afterglow under a pressure of 0.9 Torr.

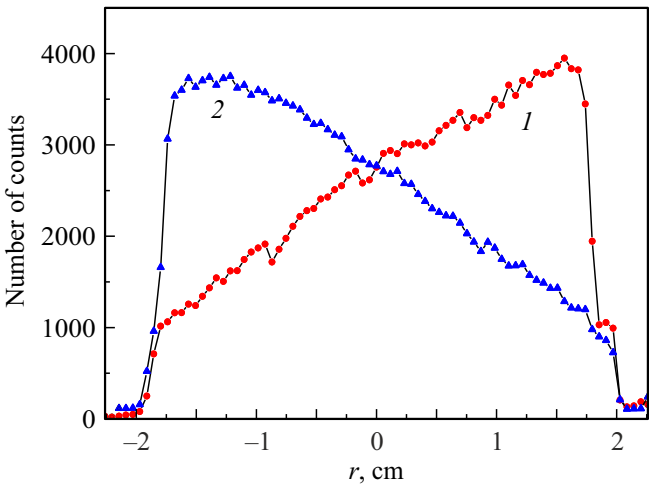

Figure 3. Radial distribution of plasma glow at a wavelength of 585.2 nm in the first (*1*) and the second (*2*) half-waves of the discharge current.

the second half-wave. Measurements were performed with gating of the photomultiplier signal within the time intervals indicated in Fig. 2. Thus, an almost Π-shaped glow distribution over the tube radius is typical of the early afterglow (curve *3* in Fig. 4, which corresponds to the third gating interval in Fig. 2). Owing to higher diffusion modes, this distribution transforms quickly into a glow that is close to the one typical of a steady-state low-pressure gas discharge.

Under higher pressures, the glow in a barrier discharge of this configuration is „pushed“ to the tube walls in a much more marked fashion and remains this way over a protracted period of time at the decay stage [11]. Note that the glow in Fig. 2 is typical of the mechanism of excitation by an electron impact. In the considered conditions, of which the smallness of density of neon atoms is a crucial one, a glow similar to the one in Fig. 2 is demonstrated only by the lines of a helium atom and neon lines with an excitation potential exceeding considerably the energy of state $He^*(2^1S_0)$ (this excludes the excitation transfer mechanism). The intensities of all the other spectral lines in the 350–750 nm range in the early afterglow follow the variation of population $[He^*(2^1S_0)](t)$.

Figure 5 shows a fragment of the DBD afterglow spectrum for the He–Ne mixture under pressures of 0.7 and 0.003 Torr, respectively. Measurements were performed in the photon count mode at 1024 points over the spectrum with the PMT signal gated by 80 μs pulses delayed by 20 μs relative to $t = 0$ (Fig. 2). The 632.8 nm line (transition $2p_4 \leftarrow 3s_2$) and the lines of transitions from the $2p_4$ level (609.6 and 594.5 nm) are indicated in the upper part of Fig. 5. It is evident that the 632.8 nm line of the He–Ne laser is one of the brightest ones in decaying plasma. The presentation of data in logarithmic scale allows one to estimate the degree of spectral purity of He–Ne plasma emission by examining the H_α line of atomic hydrogen.

As is known [5], $2p^55s$ levels in an active medium based on DC plasma are populated via a thoroughly studied process of excitation transfer in collisions

$$He(2^1S_0) + Ne \rightarrow He + Ne^*(3s_i), \qquad (1)$$

According to the results of experiments [14–18], the room-temperature cross section of this process for $3s_2$ is $2 \cdot 10^{-16}$–$4 \cdot 10^{-16}$ cm^2 (rate constant $k_{Ne} \approx 4 \cdot 10^{-11}$ cm^3/s). It turns out that this mechanism of production of excited neon atoms is also dominant at the initial DBD afterglow stage. This is confirmed by the data in Fig. 6, where the equivalence between temporal variations of the $[He(2^1S_0)]$ density and intensities of lines of transitions from levels of the $2p^55s$ (632.8 nm), $2p^54d$ (576.4 nm), $2p^54p$ (352.0 nm), and $2p^53p$ configurations is demonstrated. A change in the excitation mechanism is typical of lines originating from levels of the $2p^53p$ (585.2 nm in Fig. 6) configuration positioned below the $He(2^3S_1)$ metastable level on a scale of excitation energies: process (1) in the early afterglow gives way to a similar process involving a $He(2^3S_1)$ helium atom that remains in the afterglow for a much longer period of time. Recombination radiation is hard to notice in these conditions against the background of the excitation transfer mechanism. Its contribution to the afterglow may be estimated by examining the late stage of the 632.8 nm intensity (Fig. 6).

In the considered conditions with a low neon density (several mTorr), the $He(2^1S_0)$ state is destroyed in the afterglow primarily via collisions

$$He(2^1S_0) + e \rightarrow He(2^3S_1) + e + E_{kin}. \qquad (2)$$

The rate constant of process (2) is known ($k_e \approx 4 \cdot 10^{-7}$ cm^3/s [19]) and depends only weakly on the mean energy of electrons [20] that varies in the early afterglow. This allows one estimate fairly accurately

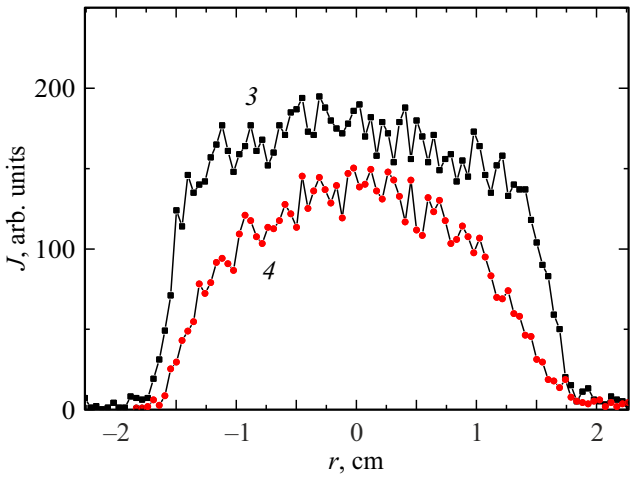

Figure 4. Radial distribution of plasma radiation at a wavelength of 585.2 nm in the afterglow: *3* — gating interval 3 (Fig. 2), *4* — gating interval with a duration of 20 μs, delayed by 20 μs relative to $t = 0$ (Fig. 2).

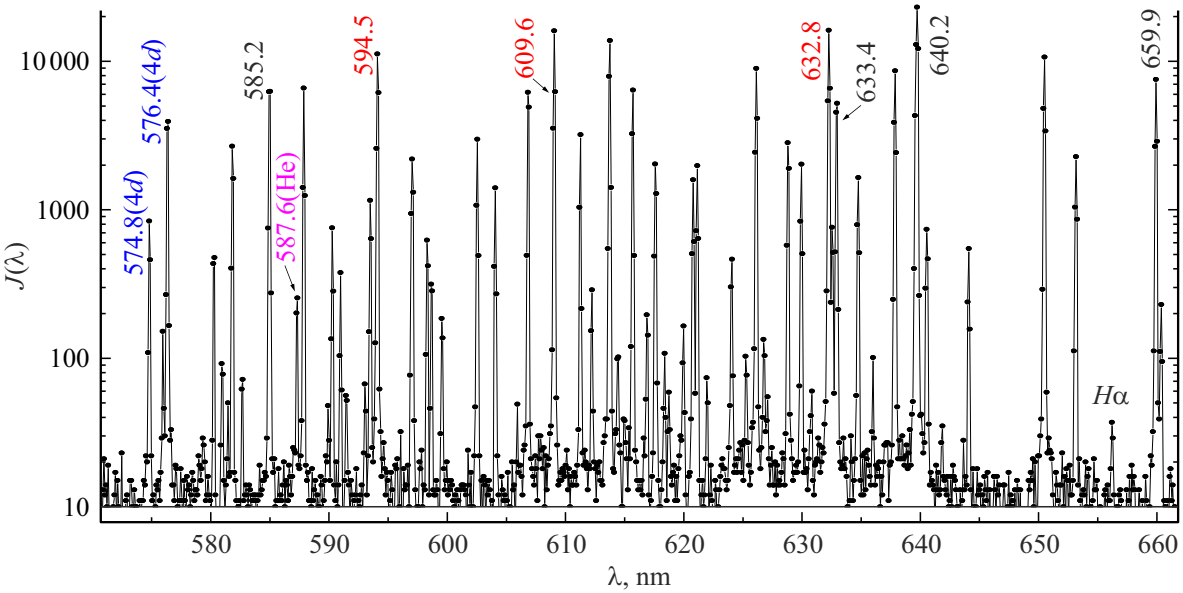

Figure 5. A fragment of the DBD afterglow spectrum at $P_{He} = 0.7$ Torr, $P_{Ne} = 0.003$ Torr.

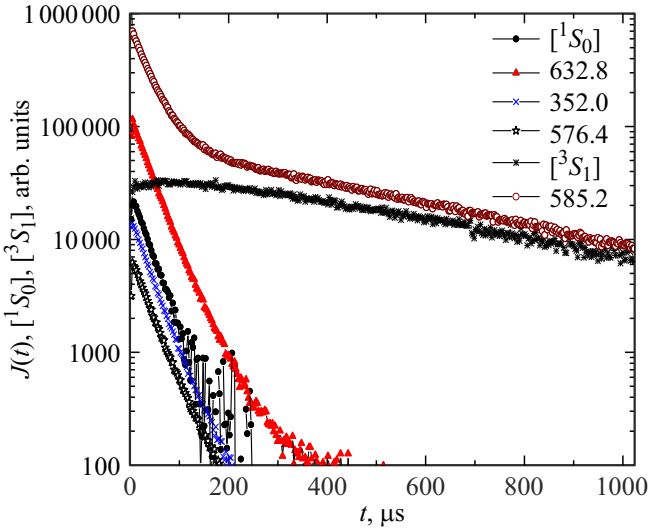

Figure 6. Intensities of spectral lines and densities of metastable helium atoms $[He^*(2^1S_0)]$ and $[He^*(2^3S_1)]$ in the afterglow. $P_{He} = 0.7$ Torr, $P_{Ne} = 0.003$ Torr. The values of $[He^*(2^1S_0)]$ and $[He^*(2^3S_1)]$ densities at the end of the discharge are $5 \cdot 10^{10}$ and $8 \cdot 10^{10}$ cm^{-3}, respectively.

the density of electrons of a decaying plasma of the He–Ne mixture based on the results of spectroscopic measurements of the $[He^*(2^1S_0)](t)$ value. The data in Figs. 2–6 correspond to an electron density at the beginning of the afterglow of $\approx 6 \cdot 10^{10}$ cm^{-3}.

In accordance with the selection rules, nine spectral lines originating from the $3s_2$ level of a neon atom connect it to all levels of the $2p^5 3p$ configuration (except for $2p_9$). Table 1 lists the relative populations of $3s_2$ and $2p_i$ levels calculated based on line intensities in the afterglow with

Table 1. Populations of $2p_i$ levels relative to $3s_2$ determined based on intensities J_i (in numbers of photoelectrons) of the brightest lines of a neon atom in the afterglow under a helium and neon pressure of 0.7 and 0.003 Torr, respectively. J is the total angular momentum of the upper states of transitions

λ_i, nm	A_{ik}, 10^6 s^{-1}	J_i	$S(\lambda_i)$	$[N_i]/[N_{3s_2}]$	J
632.8 ($3s_2-2p_4$)	3.4	16000	0.78	1	1
585.2 ($2p_1-1s_2$)	61	8550	0.92	0.025	0
659.9 ($2p_2-1s_2$)	23.2	7523	0.69	0.1	1
588.2 ($2p_2-1s_5$)	11.5	6590	0.91	0.08	1
607.4 ($2p_3-1s_4$)	60	8054	0.83	0.027	0
609.6 ($2p_4-1s_4$)	18.1	16300	0.87	0.17	2
612.8 ($2p_5-1s_4$)	0.67	304	0.83	0.09	1
630.5 ($2p_6-1s_4$)	4.16	2040	0.78	0.1	2
638.3 ($2p_7-1s_4$)	32	8714	0.76	0.1	1
650.6 ($2p_8-1s_4$)	30	10760	0.71	0.08	2
724.5 ($2p_{10}-1s_4$)	10	3600	0.4	0.15	1

account for spectral sensitivity $S(\lambda)$ of the experimental setup:

$$[N_i] = J(\lambda_i)/(S(\lambda_i)A_{ik}).$$

Sensitivity $S(\lambda)$ of the optical circuit for radiation detection was measured with an LS-1-CAL continuous-spectrum source, which is used to calibrate the absolute spectral sensitivity in the 300–1050 nm range. Transition probabilities were taken from the NIST Database tables [21]. A well-pronounced inversion of population of the $3s_2$ level relative to all $2p_i$ levels is evident in Table 1. The degree of this inversion is minimized in the case of $2p_4$ (the lower level of the 632.8 nm line). With such populations, light amplification (with the total angular momenta of states

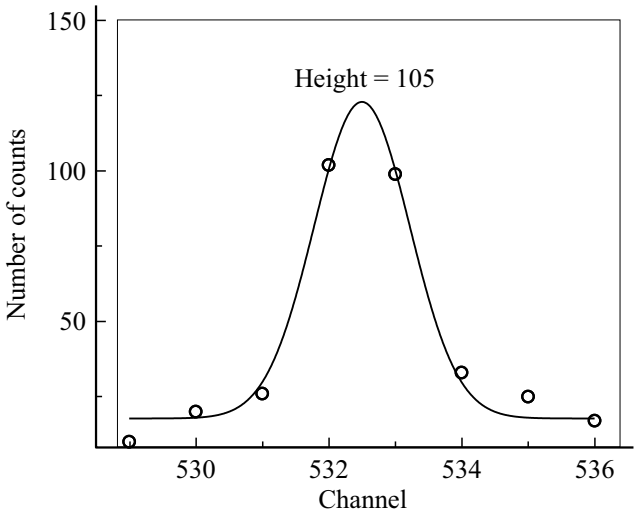

Figure 7. A fragment of the afterglow spectrum at the 615.0 nm line (transition $3p \leftarrow 4d$).

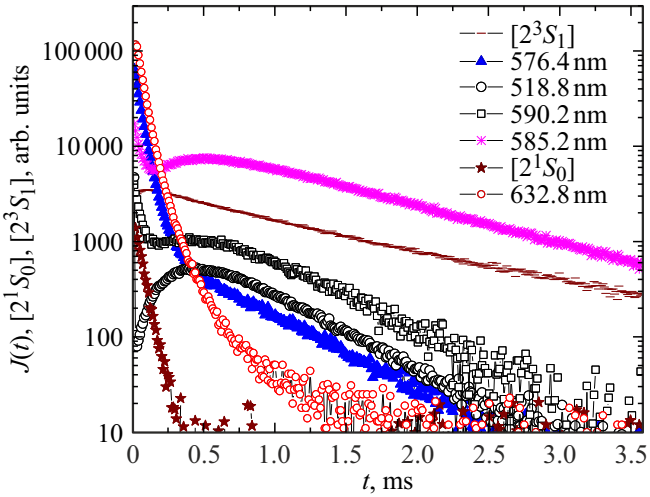

Figure 8. DBD afterglow under a helium pressure of 6.8 Torr and a neon pressure of 0.003 Torr. The density of electrons at the onset of afterglow $[e] \sim 4.5 \cdot 10^{10}\,\mathrm{cm}^{-3}$. The intensity of the 518.8 nm line is enhanced four-fold.

Table 2. Relative populations of levels $2p^5 5s$ determined based on the intensities of lines (specified in parentheses) in the afterglow and the probabilities of transmissions taken from the NIST Database [21]

Levels $2p^5 5s$	This study	[21]
$3s_2$ (632.8)	1	1
$3s_3$ (606.5)	0.004	0.005
$3s_4$ (621.4)	0.12	0.11
$3s_5$ (618.3)	0.12	0.10

taken into account) is possible at all lines of the $2p_i \leftarrow 3s_2$ transitions.

To determine the $[2p_i]$ populations, we chose the lines of transitions to the least populated (and, consequently, the least susceptible to absorption) resonance $1s_2$ and $1s_4$ levels of a neon atom. However, it follows from the $[2p_2]/[3s_2]$ ratios determined for two lines at 659.9 and 588.2 nm (the latter line ends at the lower metastable $1s_5$ level) that the absorption of radiation in this experiment does not lead to any significant errors.

Since the intensities were measured in a discrete set of points distributed over the spectrum, the values of $J(\lambda_i)$ were determined by approximating the corresponding spectrum section by a Gaussian function and calculating the intensity at the maximum of the curve. An example of this procedure is presented in Fig. 7.

It should be noted that the relative populations of levels $2p^5 5s$ of a neon atom in the afterglow in this experiment turned out to be virtually identical to the ones determined in radically different conditions [22] of purely optical excitation of $\mathrm{He}(2^1S_0)$ atoms in a He–Ne mixture under a pressure of 0.9 and less than 0.07 Torr for He and Ne. This follows from the data in Table 2, which also indicate that fundamentally non-equilibrium population distributions are established in both cases. The latter fact suggests that helium plays a negligible role in the collisional „mixing“ of excited states of a neon atom in both experiments.

Similar measurements performed under pressures of 6.8 Torr and 3 mTorr of mixture components and at $[e] \sim 4.5 \cdot 10^{10}\,\mathrm{cm}^{-3}$ revealed that the degree of population inversion decreases at a higher helium pressure and vanishes completely following the transition to the stage of recombination population of levels. This is demonstrated in Fig. 8, where the afterglow evolution is presented. The densities of helium and neon atoms in these conditions are sufficient to form molecular ions $HeNe^+$ and Ne_2^+ in triple collisions:

$$Ne^+ + He + He \rightarrow HeNe^+ + He, \quad (3a)$$

$$HeNe^+ + Ne \rightarrow Ne_2^+ + He, \quad (3b)$$

which recombine with electrons

$$HeNe^+ + e \rightarrow Ne^* + He, \quad (4a)$$

$$Ne_2^+ + e \rightarrow Ne^* + Ne \quad (4b)$$

to populate efficiently all states of a neon atom with energies lower than the one of the ground vibrational level $v = 0$ of a $HeNe^+$ ion [8,9,23].

Since energy $E(v = 0) \sim 21$ eV [23,24], the entire set of excited states of a Ne atom considered in this study (from $2p^5 6s$ (or from $2p^5 4p$ for a Ne_2^+ ion [25]) and further down the excitation energy scale) emerges directly in reactions (4) or due to cascade transitions in plasma. At the same time, levels $2p^5 6s$ are already unavailable for excitation transfer process (1). This is indicated by the afterglow at the 518.8 nm line of transition $2p^5 3p \leftarrow 2p^5 6s$ (Fig. 8) that is free from the influence of metastable helium atoms $\mathrm{He}(2^1S_0)$. It can be seen from Fig. 8 that the contribution of recombination radiation relative to excitation transfer (1)

may vary widely even in the case of levels of the same $2p^5 4d$ configuration: the ratio of intensities of the 590.2 nm (the upper level energy is 20.804 eV) and 576.4 nm lines (20.705 eV) increases by almost two orders of magnitude when the population mechanism changes in the afterglow. This is representative of the resonance nature of process (1) (the excitation energy of state $He(2^1S_0)$ is 20.62 eV), while electron–ion recombination evidently has a different nature.

In our view, the above data suggest that it is reasonable to discuss the use of cylindrical DBD in generation of plasma of an active medium of a He–Ne laser. In the present study, we limited ourselves to analyzing the emission of plasma with electron density $[e] < 10^{11}$ cm^{-3}. However, it was found experimentally that it is easy to raise $[e]$ (and, consequently, the densities of metastable helium atoms) by an order of magnitude using the discharge supply circuit from Fig. 1 even in a tube with a radius of 1.9 cm, which is far from being the optimum one for laser applications. This supply circuit provides two simple ways to do that: one may either increase pulse duration t_p at the transistor gate and thus raise the energy transferred to the secondary winding or, as was demonstrated in our experiment, increase the discharge frequency by shortening the afterglow stage. The following two obvious advantages of the discharge circuit in Fig. 1 should be noted: its electrodeless nature, which makes the operational life of a discharge tube almost infinite, and the simplicity of the electrical circuit, which contains only two semiconductor elements.

The specific features of kinetics of helium atoms in metastable states $He(2^1S_0)$ and $He(2^3S_1)$, which are present in the afterglow in appreciable densities within different time intervals (Figs. 6, 8), allow one to predict the capacity for generation of both the complete set of laser lines and the 1.15 μm line associated with long-lived $He(2^3S_1)$ atoms only. The latter line was not observed in our experiments, but we do not see the reasons why population inversion should be lacking in the afterglow in the $4s-3p$ level system.

Concluding the discussion of He–Ne plasma properties, we note, as an addition to the phenomenon [10] mentioned in the introductory section, another aspect that is quite intriguing for an object that has been studied so extensively and for so long. The substance of the matter (see details in [26]) is related to the well-known [27] feature of the process of dissociative recombination of molecular helium ions He_2^+

$$He_2^+ + e \rightarrow He^* + He \qquad (5)$$

that proceeds in decaying plasma and involves vibrationally excited molecular ions $He_2^+(v)$ with $v \geq 3$ only. The most populated lower ion states are thus excluded from (5), making the contribution of the ion to plasma decay insignificant, and the belief established since the publication of [28], which holds that the rates of vibrational relaxation of molecular ions in intrinsic gas are high, predetermines the impossibility of experimental observation of plasma emission related to (5) against the background of collisional–radiative recombination of He^+ ions:

$$He^+ + e + e \rightarrow He^* + e. \qquad (6)$$

The dependence of the rate of this process on the electron temperature (it is proportional to $T_e^{-4.5}$ in the case of purely collisional kinetics of an excited electron) is much stronger [29,30,32] than the corresponding dependence for the rate of dissociative recombination (from $T_e^{-0.5}$ to $T_e^{-1.5}$ [31]). This difference provides an opportunity to make a qualitative distinction between the recombination mechanisms of production of excited atoms by observing the response of emission of decaying plasma to pulsed „heating“ of electrons. Some of the results of such an experiment with a pulsed high-frequency field are presented in Fig. 9. The fundamental difference between the 503.8 nm (the energy of the upper $5d$ level is 21.015 eV, and the binding energy of an excited electron is 0.55 eV) and 585.2 nm (the energy of the upper $3p$ level is 18.96 eV) lines in terms of temporal behavior and the response to electron „heating“ is evident. The population of the considered $5d$ level, which is beyond the reach of processes (1) and (4), is attributable to the collisional–radiative recombination of Ne^+ ions with a strong dependence of the rate on T_e that is typical of this process. At the same time, the population of $3p$ levels is related (with the sole exception of the earliest afterglow) to processes (4). When it comes to one of the brightest helium lines at 587.6 nm (the energy of the upper $3d$ level is 23.07 eV, and the binding energy of an excited electron is 1.52 eV), its intensity in the collisional–radiative recombination model should respond to T_e variations in the same way as the 503.8 nm line of a neon atom does, since the rates of the process in helium and neon are the same and are proportional to $T_e^{-4.5}$ [31] at an electron density close to 10^{11} cm^{-3}. The latter assertion is inconsistent with the experimentally observed features of behavior of the 587.6 nm line. It is evident that more accurate data on

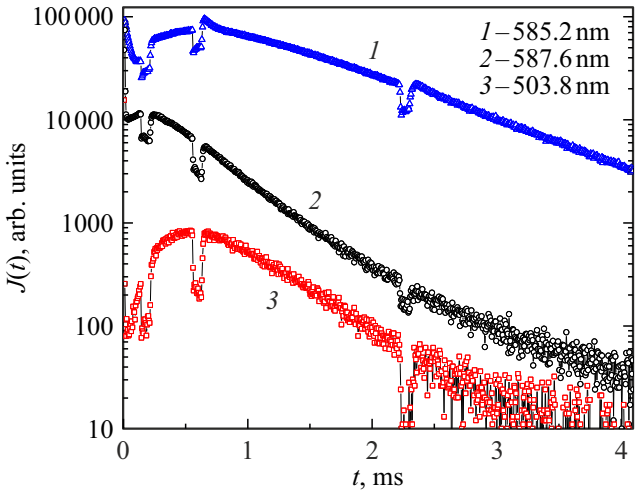

Figure 9. Intensities of spectral lines of helium (587.6 nm) and neon in the afterglow. $P_{He} = 0.7$ Torr, $P_{Ne} = 0.003$ Torr, and the electron density at the onset of afterglow is $[e] \sim 9 \cdot 10^{10}$ cm^{-3}.

the mechanisms of electron–ion recombination as sources of excited atoms in helium plasma are needed to interpret these features.

Conclusions

Helium–neon plasma of an extended low-pressure barrier discharge was examined by kinetic spectroscopy in the wavelength range of 350–750 nm to identify the conditions of formation of inverse population of excited levels of a neon atom in decaying plasma. The temporal characteristics and spectra of plasma emission in the discharge and the afterglow under a helium pressure of 0.7 and 6.7 Torr and a neon pressure of 3 mTorr at an electron density lower than $10^{11}\,\mathrm{cm}^{-3}$ were examined. Populations $[\mathrm{He}(2^1S_0)](t)$ and $[\mathrm{He}(2^3S_1)](t)$ of metastable states of a helium atom were determined based on the variations of light absorption at transitions to these states, and the equivalence between temporal variations of population $[\mathrm{He}(2^1S_0)](t)$ and the intensities of spectral lines of transitions $3p \leftarrow 5s$, $3p \leftarrow 4d$, $3s \leftarrow 4p$, and $3s \leftarrow 3p$ at the early afterglow stage at $t < 150\,\mu$s was demonstrated. A well-pronounced population inversion of the upper level of the $2p^5 5s$ configuration ($3s_2$ in the Paschen notation) relative to all levels of the $2p^5 3p$ configuration is observed at this stage. At $t \geq 150\,\mu$s, plasma emission is formed primarily by the $3s \leftarrow 3p$ transition lines, the intensities of which vary with time in the same way as $[\mathrm{He}(2^3S_1)](t)$. When the helium pressure increases, the afterglow spectrum is enriched with emission produced due to the dissociative recombination of $HeNe^+$ and Ne_2^+ ions with plasma electrons; however, this mechanism does not yield population inversion. The feasibility of application of a cylindrical DBD with electrodes positioned along the side surface of a discharge tube as a plasma source for an active medium of a He–Ne laser was discussed with reference to experimental data.

Conflict of interest

The author declares that he has no conflict of interest.

References

[1] R. Brandenburg. Plasma Sources Sci. Technol., **26** (5), 053001 (2017). https://doi.org/10.1088/1361-6595/aa6426
[2] U. Kogelschatz. Plasma Chem. Plasma Proc., **23** (1), 1 (2003).
[3] D. Gellert, U. Kogelschatz. Appl. Phys. B, **52** (1), 14 (1991).
[4] A. Javan, W.R. Jr. Bennett, D.R. Herriott. Phys. Rev. Letters, **6** (3), 106 (1961). DOI: 10.1103/PhysRevLett.6.106
[5] A.D. White, J.D. Rigden. Proceedings of the IRE, **50** (7), 1697 (1962). DOI: 10.1109/JRPROC.1962.288157
[6] L. Allen, D.G.C. Jones. Principles of Gas Lasers. London, Butterworths, 1967.
[7] A.Z. Devdariany, A.L. Zagrebin, K. Blagoev. Annales De Physique, **17** (5), 365 (1992).
[8] V.A. Ivanov, A.S. Petrovskaja, Yu.E. Skoblo, Opt. Spectrosc., **117** (6), 896 (2014). DOI: 10.1134/S0030400X14120108.
[9] V.A. Ivanov, A.S. Petrovskaja, Yu.E. Skoblo. Opt. Spectrosc., **123** (5), 692 (2017). DOI: 10.1134/S0030400X17110091.
[10] V.A. Ivanov, Yu.E. Skoblo. Opt. Spectrosc., **127** (5), 820 (2019). DOI: 10.1134/S0030400X19110110
[11] V.A. Ivanov. Opt. Spectrosc., **126** (3), 167 (2019). DOI: 10.1134/S0030400X1903007X.
[12] V.A. Ivanov. Plasma Sources Sci. Technol., **29** (4), 045022 (2020). https://doi.org/10.1088/1361-6595/ab7f4c
[13] V.A. Ivanov. J. Phys. B: At. Mol. Opt. Phys., **31**, 1765 (1998). http://iopscience.iop.org/0953-4075/31/8/025.
[14] E.E. Benton, E.E. Ferguson, F.A. Matson, W.W. Robertson. Phys. Rev., **128** (1), 206 (1962).
[15] O.P. Botchkova, Yu.A.Tolmahev, S.E. Frish. Opt. Spectrosc., (USSR) **23**, 500 (1967).
[16] C.R. Jones, F.E. Niles, W.W. Robertson. J. Appl. Phys., **40**, 3967 (1969).
[17] J.T. Massey, A.G. Shultz, B.F. Hochheimer, S.M. Cannon. J. Appl. Phys., **36**, 658 (1965).
[18] V.P. Chebotaev, L.S. Vasilenko. Opt. Spectrosc., **20**, 313 (1966).
[19] A.V. Phelps. Phys. Rev., **99**, 1307 (1955).
[20] V.A. Ivanov, A.S. Prikhod′ko, Yu.E. Skoblo. Opt. Spectrosc., **70**, 297 (1991).
[21] NIST Atomic Spectra Database Lines Form [Electronic source]. URL: https://physics.nist.gov/PhysRefData/ASD/lines_form.html
[22] H.K. Haak, B. Wittig, F. Stuhl. Z. Naturforsch., **35A**, 1342 (1980).
[23] V.A. Ivanov, A.S. Petrovskaja, Yu.E. Skoblo, JETP, **128**, 767 (2019). DOI: 10.1134/S1063776119030051.
[24] X.J. Liu, Y.Z. Qu, B.J. Xiao, C.H. Liu, Y. Zhou, J.G. Wang, R.J. Buenker. Phys. Rev. A **81** (2), 022717 (2010). DOI: 10.1103/PhysRevA.81.022717
[25] V.A. Ivanov, S.V. Gordeev, Yu.E. Skoblo. Opt. Spectrosc., **127** (3), 418 (2019). DOI: 10.1134/S0030400X19090133.
[26] V.A. Ivanov, Yu.E. Skoblo. Opt. Spectrosc. **127** (6), 962 (2019). DOI: 10.1134/S0030400X19120087.
[27] R.S. Mulliken. Phys. Rev., **136** (4A), 962 (1964). DOI: 10.1103/PhysRev.136.A962
[28] D.R. Bates. Comments Atom. Mol. Phys., **5**, 89 (1976).
[29] A.V.Gurevich, L.P. Pitaevskii. Sov. Phys. JETP, **19** (4), 870 (1964).
[30] D.R. Bates, A.E. Kingston, R.W.P. McWhirter. Proc. Roy. Soc. (London), **A267**, 297 (1962). https://www.jstor.org/stable/2414257
[31] V.A. Ivanov. Sov. Phys. Usp., **35** (1), 17 (1992). DOI: 10.3367/UFNr.0162.199201b.0035. [V.A. Ivanov. Sov. Phys. Usp., (1), 17 (1992). DOI: 10.1070/PU1992v035n01ABEH002192].
[32] J. Stevefelt., J. Boulmer, J.-F. Delpech . Phys. Rev. A **12** (4), 1246 (1975). DOI: 10.1103/PhysRevA.12.1246